

# Surface features of graft-type polymer electrolyte membranes determined by tapping mode atomic force microscopy analysis

Nguyen Nhat Kim Ngan<sup>1,2</sup>, Nguyen Manh Tuan<sup>2,3</sup>, Nguyen Huynh My Tue<sup>2,3</sup>, Vo Thi Kim Yen<sup>2,3</sup>, Dinh Tran Trong Hieu<sup>2,3</sup>, Hoang Anh Tuan<sup>2,3</sup>, Tran Ngoc Tien Phat<sup>2,3</sup>, Lam Hoang Hao<sup>2,3</sup>, Nguyen Thanh Ta<sup>2,3</sup>, Doan Thi Kim Ngan<sup>2,3</sup>, Tran Duy Tap<sup>\*</sup>



Use your smartphone to scan this QR code and download this article

## ABSTRACT

**Introduction:** Polymer electrolyte membrane fuel cells (PEMFCs) are promising renewable energy technologies that are increasingly used in commercial transportation, stationary, and portable devices. In PEMFCs, the surface nature of PEMs plays a key role in the interfacial degradation of membrane–electrolyte assembly and proton conductance and thus strongly impacts the performance and stability of PEMFCs. Consequently, the objective of this work was to investigate the surface features of graft-type poly(styrenesulfonic acid) (PSSA)-grafted poly(ethylene-co-tetrafluoroethylene) polymer electrolyte membranes (ETFE-PEMs) by tapping mode atomic force microscopy (TM-AFM). **Methods:** ETFE-PEMs were prepared via preirradiation-induced grafting of styrene onto an ETFE film followed by sulfonation. All the ETFE-PEMs and their precursor films (original ETFE and polystyrene (PS)-grafted ETLEs) were characterized via TM-AFM. **Results:** In the grafting and sulfonation process, partially grafted PS and PSSA chains accumulate on the sample surface at a low grafting degree (GD) of 21%, and more graft chains diffuse into the bulk of the membranes at higher GDs of 36 and 57%. The polystyrene grafts are immiscible mostly with the amorphous phase of the pristine ETFE film, leading to the formation of a new amorphous phase containing only PS grafts. Sulfonation resulted in microphase separation between the backbone of ETFE and the side chain of PSSA, but the final surface morphology of the membranes can be determined at the grafting step. **Conclusions:** The surface morphology characteristics are more or less ascertained during the grafting process but not during the sulfonation process. The PSSA grafts of ETFE-PEMs are dispersed on the membrane surface, favoring the connection of ionic domains and leading to an increase in proton conductance on the membrane surface. These findings suggest that ETFE-PEMs have advantages in terms of membrane–electrode interfacial properties for PEMFC applications because of their low accumulated surface area and low GD.

**Key words:** ETFE-PEM, polymer electrolyte membranes, surface feature, AFM

<sup>1</sup>Faculty of Physics and Engineering Physics, University of Science, Ho Chi Minh City, Vietnam

<sup>2</sup>Viet Nam National University, Ho Chi Minh City, Vietnam

<sup>3</sup>Faculty of Materials Science and Technology, University of Science, Ho Chi Minh City, Vietnam

## Correspondence

Tran Duy Tap, Email: tdtap@hcmus.edu.vn

## History

- Received: 2024-09-30
- Revised: 2024-12-11
- Accepted: 2024-12-25
- Published Online: 2024-12-31

## DOI :



## Copyright

© VNUHCM Press. This is an open-access article distributed under the terms of the Creative Commons Attribution 4.0 International license.



## 1 INTRODUCTION

2 The polymer electrolyte membrane fuel cell (PEMFC)  
3 has attracted much attention for applications in trans-  
4 portation, stationary, and portable devices because of  
5 its high energy efficiency (40–60%) and lack of gas  
6 emission. This application is expected to address pol-  
7 lutant emissions and thus reduce the impact of cli-  
8 mate change<sup>1</sup>. The polymer electrolyte membrane  
9 (or proton exchange membrane) (PEM) is the key  
10 component of a PEMFC because its ionic conductiv-  
11 ity, mechanical strength, and thermal and chemical  
12 stability are significantly related to the performance  
13 and durability of the cell. Perfluorosulfonic acid  
14 membranes such as Nafion are the state-of-the-art  
15 advanced materials for PEMs, but their limitations,  
16 such as high production cost and low performance  
17 at high temperature and low relative humidity (RH),  
18 have triggered investigations of alternative polymer

19 electrolyte membranes to replace Nafion<sup>1</sup>. In our  
20 previous works<sup>2–18</sup>, we reported the synthesis and  
21 characterization of poly(styrenesulfonic acid)-grafted  
22 poly(ethylene-co-tetrafluoroethylene) polymer elec-  
23 trolyte membranes (ETFE-PEMs) within a wide range  
24 of grafting degrees (GDs) of 0–125%, corresponding  
25 to an ion exchange capacity (IEC) of 0–3.3 mmol/g via  
26 gamma-ray irradiation-induced grafting of styrene  
27 onto an ETFE film (grafted-ETFE) and subsequent  
28 sulfonation of the grafted film. Compared with other  
29 fully or partially fluorinated graft-type PEMs<sup>19–21</sup>  
30 or Nafion membranes<sup>9,10,15,16</sup>, ETFE-PEMs exhibit  
31 higher or comparable proton conductivities, mechan-  
32 ical integrity and thermal stability. In particular,  
33 ETFE-PEMs with high IECs (> 2.7 mmol/g) show  
34 greater conductivity at 30% RH and competitive ten-  
35 sile strength at 100% RH and 80 °C than the commer-  
36 cial Nafion-212 membrane<sup>15</sup>.

**Cite this article :** Ngan N N K, Tuan N M, Tue N H M, Yen V T K, Hieu D T T, Tuan H A, Phat T N T, Hao L H, Ta N T, Ngan D T K, Tap T D. **Surface features of graft-type polymer electrolyte membranes determined by tapping mode atomic force microscopy analysis.** *Sci. Tech. Dev. J.* 2025; 27(4):1-10.

37 Recently, membrane–electrode assembly (MEA)  
38 failures have been observed after only a few hundred  
39 PEM operations and have been found to be closely  
40 related to the nature of the membrane surface<sup>22,23</sup>.  
41 The inferior interfacial properties of MEAs have  
42 been recognized to be associated with backbone and  
43 functional chain degradation and crack development.  
44 For example, concentrated PSSA grafts on the  
45 surface of poly(styrene sulfonic acid) (PSSA)-grafted  
46 poly(tetrafluoroethylene-coperfluorovinyl ether)  
47 polymer electrolyte membranes (PFA-PEMs) and  
48 PSSA-grafted poly(tetrafluoroethylene) polymer  
49 electrolyte membranes (PTFE-PEMs) were observed  
50 to decompose within 50 h in fuel cells running<sup>24–26</sup>.  
51 Moreover, the low or high functional graft distri-  
52 bution on the membrane surface resulted in low  
53 conductance and surface fractures, respectively<sup>27,28</sup>.  
54 However, there are still limitations in the detailed  
55 and systematic evaluation of the surface features of  
56 ETFE-PEMs<sup>2,5</sup>, although these limitations are quite  
57 important for their performance in PEMFCs.  
58 Tapping mode atomic force microscopy (TM-AFM) is  
59 a potential method for investigating the surface mor-  
60 phology of membranes because it allows us to observe  
61 high-resolution topographic images and avoid any  
62 surface dragging effects of tips on surface sampling<sup>29</sup>.  
63 In TM-AFM analysis, common parameters such as  
64 surface roughness ( $S_a$ ), root-mean-square roughness  
65 ( $S_q$ ), and maximum spike-to-valley height roughness  
66 ( $S_z(P-V)$ ) are often used to describe the surface ar-  
67 chitecture in the vertical dimension. Since these pa-  
68 rameters do not show any information in the hori-  
69 zontal direction, the additional shape parameter of  
70 skewness ( $S_{kew}$ ) is chosen to provide missing infor-  
71 mation in the horizontal direction. This combination  
72 provides a comprehensive understanding of the sur-  
73 face architecture of membranes. The aim of this work  
74 was to investigate the change in the surface morphol-  
75 ogy of ETFE-PEMs through the preparation proce-  
76 dure and with the degree of grafting via AFM analy-  
77 sis. As the structural features of the final polymer elec-  
78 trolyte membrane (ETFE-PEM) are highly dependent  
79 on those of the pristine polymer and grafted polymer  
80 films, TM-AFM measurements of the pristine ETFE  
81 and grafted-ETFE films were also conducted.

## 82 EXPERIMENTAL

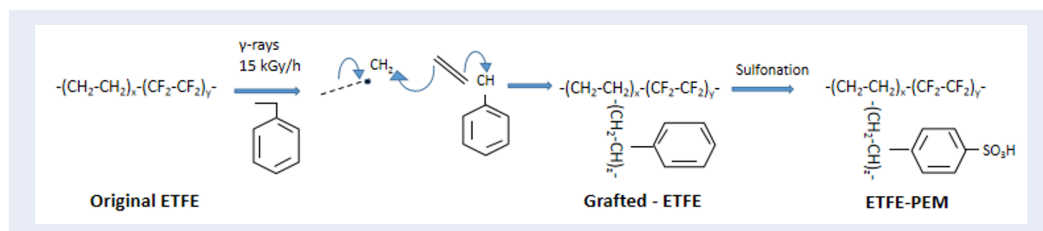
### 83 Materials

84 Commercial 50- $\mu$ m-thick ETFE films (or Tefzel  
85 films) were purchased from AGC Ltd., Japan. Fur-  
86 thermore, other chemical substances (i.e., styrene,  
87 1,2-dichloroethane, hydrogen peroxide, acetone,

88 toluene, and chlorosulfonic acid) were obtained from  
89 Wako Pure Chemical Industries, Ltd., Japan. In  
90 this work, all the chemical substances were used as  
91 received (i.e., without further treatment).

### 92 Preparation of graft-type ETFE-PEMs

93 The general procedures for the preparation and chem-  
94 ical structures of ETFE, grafted-ETFE, and ETFE-  
95 PEM are depicted in Scheme 1. The preparations were  
96 similar to those comprehensively described in our  
97 previous works<sup>11,15</sup>. Accordingly, the present study  
98 is briefly outlined as follows. The ETFE films were ir-  
99 radiated by g-rays emitted from a  $\text{Co}^{60}$  source under  
100 and an argon atmosphere. The energies of the gamma  
101 rays are approximately 1.17 and 1.33 MeV. These en-  
102 ergies are high enough for the occurrence of photo-  
103 electric, Compton, and pair production effects within  
104 the irradiated ETFE films at the same time. These ef-  
105 fects can generate a large number of secondary elec-  
106 trons, which in turn induce many sequential physical  
107 interactions (coastal interactions) to create free rad-  
108 icals. The absorbed dose and dose rate were 15 kGy  
109 and 15 kGy/h, respectively. This irradiation dose is  
110 expected to generate free radicals but does not mod-  
111 ify the microstructures within the irradiated films<sup>4</sup>.  
112 These free radicals serve as active sites for the graft-  
113 ing process. The irradiated films were then immersed  
114 in a styrene/toluene mixture at different concentra-  
115 tions and different time courses at 60 °C for graft  
116 polymerization to obtain polystyrene-grafted ETFE  
117 films. During the grafting process, the PS chains  
118 are expected to diffuse through the amorphous phase  
119 until the grafting occurs mostly at the crystalline–  
120 amorphous interfaces (where the free radicals can last  
121 much longer than those in the amorphous regions,  
122 where the free radicals vanish rapidly). The degree  
123 of grafting (GD) is determined via the following for-  
124 mula:  $\text{GD} (\%) = 100 \times (W_g - W_0) / W_0$ , where  $W_0$   
125 and  $W_g$  are the masses of the sample before and after  
126 the grafting step, respectively. The grafted films were  
127 soaked in a 0.2 M chlorosulfonic acid solution in 1,2-  
128 dichloroethane at 50 °C (approximately 6 hours) for  
129 sulfonation to obtain the graft-type ETFE-PEMs<sup>11,15</sup>.  
130 Note that the chemical structures of the grafted ETLs  
131 and ETFE-PEMs were confirmed by Fourier trans-  
132 form infrared (FT-IR) spectroscopy<sup>11</sup> and X-ray pho-  
133 toelectron spectroscopy (XPS) analysis<sup>5</sup>. Specifically,  
134 new bands appeared at 1492 and 1600  $\text{cm}^{-1}$  (skele-  
135 tal in-plane deformation of the conjugated C=C of the  
136 benzene ring), and new bands emerged at 756 and 698  
137  $\text{cm}^{-1}$  (CH out-of-plane vibration), indicating that  
138 styrene was grafted onto the ETFE film. Moreover,



Scheme 1: **Preparation procedure and structures of graft-type ETFE-PEMs.** The samples were prepared via preirradiation-induced grafting of styrene onto the ETFE substrate to obtain the grafted-ETFE and subsequent sulfonation to obtain the ETFE-PEM. Owing to the high energy of gamma rays, the whole volume of the ETFE film is expected to be irradiated at the same time. The generated radicals within the amorphous phase vanish quickly, whereas those within the crystallites or crystallite surfaces can last for a long time. Thus, the grafting is assumed to be at the amorphous–crystalline interface<sup>9,17</sup>.

139 new bands at 840 and 607  $\text{cm}^{-1}$  (stretching vibration  
 140 of S=O) appear after sulfonation, which suggests that  
 141 the grafted-ETFE was sulfonated successfully to cre-  
 142 ate the ETFE-PEM. XPS analysis revealed a signifi-  
 143 cant decrease in the fluorine content, which mainly  
 144 resulted from graft incorporation and the defluorina-  
 145 tion reaction during the grafting process. In addition,  
 146 an additional peak at 169.1 eV was observed, indi-  
 147 cating the existence of sulfonic acid groups ( $\text{SO}_3^-$ )  
 148 within the ETFE-PEM.

#### 149 AFM measurement

150 The AFM analyses of the original ETFE, grafted-ETFE  
 151 films, and ETFE-PEMs were carried out with a SPA-  
 152 400 instrument (Seiko Instruments, Japan) in tapping  
 153 mode under ambient conditions. The microscope was  
 154 equipped with a calibrated 20- $\mu\text{m}$ -xy-scan range and  
 155 a 10- $\mu\text{m}$ -z-scan range of the PZT scanner. All mea-  
 156 surements were conducted at room temperature us-  
 157 ing an aluminum-coated silicon tip (SI-DF40) on a  
 158 cantilever with a spring constant and resonance fre-  
 159 quencies of 31 N/m and 320 Hz, respectively. Sur-  
 160 face scanning was performed at a scan rate of 1 Hz.  
 161 The end radius of the silicon probe was approximately  
 162 10 nm. The distance from the probe to the sample  
 163 was 100 nm. Before the measurement, the samples  
 164 were cut into small pieces of  $1 \times 1 \text{ cm}^2$ , fixed to the  
 165 mica substrate with adhesive tape, and then mounted  
 166 onto the sample holder. In this study, all the images  
 167 were analyzed via Gwyddion software (version 2.49)  
 168 to determine the specific roughness parameters (i.e.,  
 169  $S_a$ ,  $S_q$ ,  $S_z(P-V)$ , and  $S_{kew}$ ) of the surface morphol-  
 170 ogy. These values were determined directly via inte-  
 171 grated routines from the height scan.  $S_a$  describes  
 172 the mean height of asperities (i.e., average surface  
 173 roughness), whereas  $S_q$  represents the standard devi-  
 174 ation of a height profile from its average height (root

mean squared surface roughness)<sup>30,31</sup>. Both the  $S_a$  175  
 and  $S_q$  parameters describe the vertical dimensions 176  
 quite well but provide no insight into the horizon- 177  
 tal dimensions of the surface architecture.  $S_z(P-V)$  178  
 and  $S_{kew}$ , which represent the distance from the high- 179  
 est to the lowest points and the irregularities on the 180  
 surface, are also used to evaluate the overall rough- 181  
 ness and asymmetry of the topography. Accordingly, 182  
 the  $S_z(P-V)$  and  $S_{kew}$  parameters are more descrip- 183  
 tive in horizontal dimensions. The line profile was 184  
 generated by selecting one line from the correspond- 185  
 ing two-dimensional image and subsequently plotting 186  
 x-translation versus height data (z-axis). Each pro- 187  
 file was plotted by using an appropriate height scale 188  
 to provide optimum resolution. These parameters are 189  
 calculated through the following expressions<sup>32</sup>: 190

$$S_a = \frac{1}{L} \int_0^L |z_i - \bar{z}| dx \quad (1)$$

$$S_q = \left[ \frac{1}{L} \int_0^L (z_i - \bar{z})^2 dx \right]^{1/2} \quad (2)$$

$$S_z(P-V) = |\max Zz + \min Zz| \quad (3)$$

$$S_{kew} = \frac{1}{LS_q^3} \int_0^L (z_i - \bar{z})^3 dx \quad (4)$$

where L is the sampling length,  $z_i$  is the height value 191  
 of point i, and  $\bar{z}$  is the average height within the scan- 192  
 ning area. The height distribution,  $r(z)$ , is also plot- 193  
 ted as the normalized probability of finding a particu- 194  
 lar height z with the origin at the lowest observed 195  
 z–height<sup>33</sup>. The distribution of surface height  $\rho(z)$  is 196  
 described in the following form: 197

$$\rho(z) = (1/S_q\sqrt{2\pi}) \exp \left[ -(z - \bar{z})^2 / 2S_q^2 \right] \quad (5)$$

## 198 RESULTS

### 199 The surface features through the prepara- 200 tion procedure

201 Figure 1 (a-i) and Table 1 show the typical 2D and  
202 3D images and height profiles of the original ETFE,  
203 grafted-ETFE, and ETFE-PEM at a GD of 21% and  
204 their corresponding surface parameters. Obviously,  
205 the  $S_a$  value of the original-ETFE (15.5 nm) is  
206 greater than that of the grafted-ETFE (8.0 nm) and  
207 ETFE-PEM (10.1 nm). The 2D and 3D images also ex-  
208 hibit the same result. Moreover, bright yellow regions  
209 corresponding to the softer domains (amorphous re-  
210 gions) are dominant over harder domains (crystallite  
211 regions) for the three samples. The straight lines in the  
212 2D images in Figure 1(d-f) represent the positions of  
213 the surface roughness profiles, as shown in Figure 1(g-  
214 i). As shown in the figures, the surface roughness  
215 profiles of the grafted-ETFE and ETFE-PEM films are  
216 more relatively homogeneous than those of the pris-  
217 tine ETFE film. The maximum surface heights  $S_z(P-  
218 V)$  of the original-ETFE, grafted-ETFE, and ETFE-  
219 PEM are 104.9, 72.2, and 81.0 nm, respectively (Ta-  
220 ble 1). Moreover, their root mean square roughness  
221 values ( $S_q$ ) and Skew values are 19.6, 10.0, and 12.6  
222 nm and 0.6, 0.3, and 0.1, respectively. All the values of  
223 the above surface parameters of the grafted-ETFE and  
224 ETFE-PEM films are lower than those of the pristine  
225 ETFE film.

### 226 Surface features with various degrees of 227 grafting

#### 228 Grafted ETLEs

229 Figure 2 shows 3D AFM images of grafted-ETFE films  
230 with different GDs ranging from 0–57%. As the de-  
231 gree of grafting increases, the formation of small graft  
232 domains containing polystyrene (PS) chains increases  
233 but at a lower rate. The  $S_a$  values at GDs of 21, 36, and  
234 57% are 15.5, 8.0, 5.9, and 8.2 nm, respectively. With  
235 similar grafting degrees, the values of  $S_q$  (10.0, 7.6, and  
236 10.1 nm),  $S_z(P-V)$  (72.2, 71.8, 73.6) and  $S_{kew}$  (0.3, 0.6,  
237 and 0.5) are obtained. Clearly, all surface parameters  
238 of the grafted-ETFE films are lower than those of the  
239 pristine ETFE film, as shown in Table 2.

#### 240 ETFE-PEMs

241 Figure 3 and Table 3 present 3D AFM images of  
242 ETFE-PEMs with GDs of 21–57% and the corre-  
243 sponding surface parameters. After sulfonation, the  
244 membranes exhibit phase separation between the hy-  
245 drophobic domain (ETFE-based film) and the hy-  
246 drophilic domain possessing groups of ionic clusters

(PSSA)<sup>9,10,15,16</sup>. As a result, the connection of ionic  
domains increases with the degree of grafting. At the  
same time, larger continuous domains are formed, es-  
pecially at GDs of 36 and 57%<sup>10</sup>. The  $S_a$  values at GDs  
of 21, 36, and 57% are 10.1, 14.2, and 23.3 nm, respec-  
tively. With similar grafting degrees, the values of  $S_q$   
(12.6, 16.4, and 28.3),  $S_z(P-V)$  (81.0, 81.4, and 169.1)  
and  $S_{kew}$  (0.1, 0.1, and 0.2) are obtained. All surface  
parameters at GDs of 21 and 36% are lower than those  
of the pristine ETFE film, whereas those at a GD of  
57% are greater.

Figure 4 depicts the height distributions of the origi-  
nal ETFE, grafted-ETFE, and ETFE-PEM with GDs of  
21–57% at a scan size of 2000 nm. The height distri-  
bution of the original ETFE is displayed by a red line,  
whereas those of the grafted-ETFE films and ETFE-  
PEMs are represented by cyan and green lines. The  
height distribution of the pristine film can be fitted by  
two Gaussian peaks with average heights of 40.1 and  
72.8 nm and FWHMs of 35.7 and 9.4 nm. In contrast,  
the height distributions of the grafted-ETFE films at  
GDs of 21, 36, and 57% can be fitted by only one Gaus-  
sian peak with average heights of 24.9, 22.5, and 22.4  
nm and FWHMs of 21.4, 16.4, and 16.3 nm, respec-  
tively. As expected, the  $z$  values of the grafted-ETFE  
films are lower than those of the original ETFE film,  
i.e., similar to the case of  $S_a$  indicated in Table 2. The  
height distribution of the ETFE-PEM at a GD of 21%  
can be fitted by a single Gaussian peak with an aver-  
age height of 38.9 nm and an FWHM of 30.4 nm.  
For the ETFE-PEMs at higher GDs, the height distri-  
bution can be fitted by two Gaussian peaks with  
average heights of 30.1 and 56.7 nm and FWHMs  
of 18.7 and 21.8 nm for a GD of 36% and average  
heights of 70.5 and 108.7 nm and FWHMs of 41.0 and  
27.8 nm for a GD of 57%. Interestingly, the  $z$  values  
of all the ETFE-PEMs are greater than those of  
the grafted-ETFE films. All the height distributions  
fit relatively high values of  $R^2$  ( $> 0.85$ ), as displayed in  
Table 4. Note that in the case of the pristine ETFE, the  
three-peak model was also fitted with the experimen-  
tal height distribution, but the third peak was very  
small in peak area and FWHM. This small peak area  
and small FWHM value are not suitable for any com-  
ponent of the surface architecture in the pristine film.  
A similar situation is found for the case of the grafted-  
ETFE with a GD of 57%. Specifically, a two-peak  
model was also fitted with the experimental height  
distribution, but the second peak was very small in  
peak area and FWHM value. This very small peak  
area and very small FWHM value do not correspond  
to any component of the surface architecture in the  
grafted ETLE film.

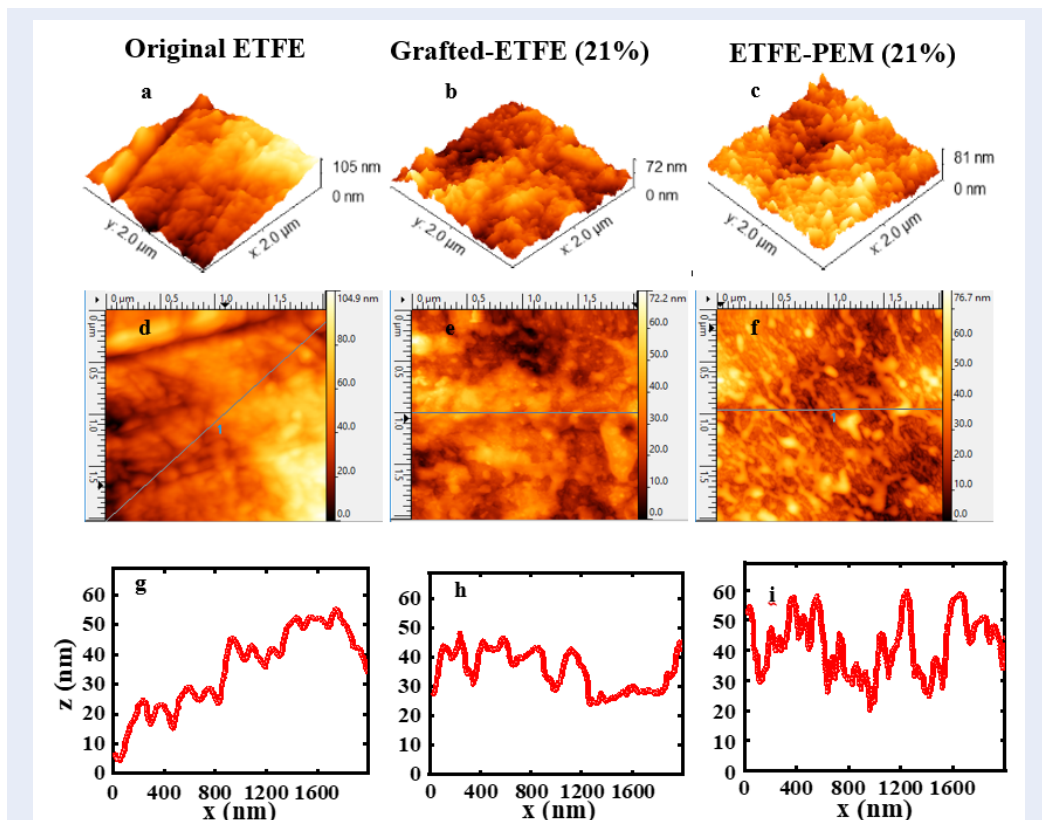


**Figure 1:** Surface features obtained through the preparation procedure at a scan size of 2000 nm. 3D (a-c) and 2D (d-f) AFM images and line profiles (g-i) of the original ETFEs, grafted-ETFEs, and ETFE-PEMs with a GD of 21%. The surface roughness profiles of the grafted-ETFE and ETFE-PEM films are more homogeneous than those of the original ETFE film.

**Table 1:** Specific roughness parameters ( $S_a$ ,  $S_q$ ,  $S_z$ (P-V), and  $S_{kew}$ ) of the original ETFE, grafted-ETFE and ETFE-PEM with a GD of 21%. The surface parameters of the grafted-ETFE and ETFE-PEM films are lower than those of the pristine ETFE film.

Sample	GD (%)	$S_a$ (nm)	$S_q$ (nm)	$S_z$ (P-V) (nm)	$S_{kew}$
Original ETFE	0	15.5	19.6	104.9	0.6
Grafted-ETFE	21	8.0	10.0	72.2	0.3
ETFE-PEM	21	10.1	12.6	81.0	0.1

**Table 2:** Specific roughness parameters ( $S_a$ ,  $S_q$ ,  $S_z$ (P-V), and  $S_{kew}$ ) of the grafted-ETFE films with GDs of 0 - 57%. The surface parameters of the grafted films are all lower than those of the pristine ETFE film. Here, the specific roughness parameters of the original ETFE are represented again for comparison.

Sample	GD (%)	$S_a$ (nm)	$S_q$ (nm)	$S_z$ (P-V) (nm)	$S_{kew}$
Original ETFE	0	15.5	19.6	104.9	0.6
Grafted-ETFE	21	8.0	10.0	72.2	0.3
Grafted-ETFE	36	5.9	7.6	71.8	0.6
Grafted-ETFE	57	8.2	10.1	73.6	0.5

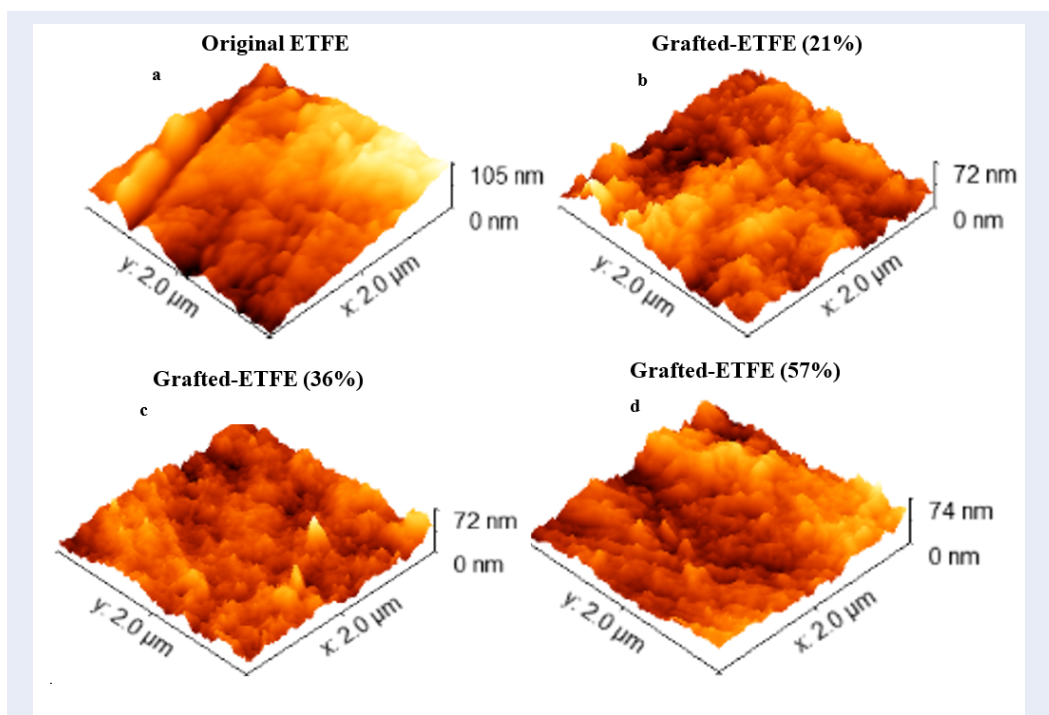


**Figure 2:** 3D surface images of the grafted-ETFE films with GDs of 0- 57% at a scan size of 2000 nm. The bright yellow regions correspond to the softer domains of the amorphous regions of the pristine ETFE and/or PS grafts. Note that the image of the original ETFE is represented again for comparison.

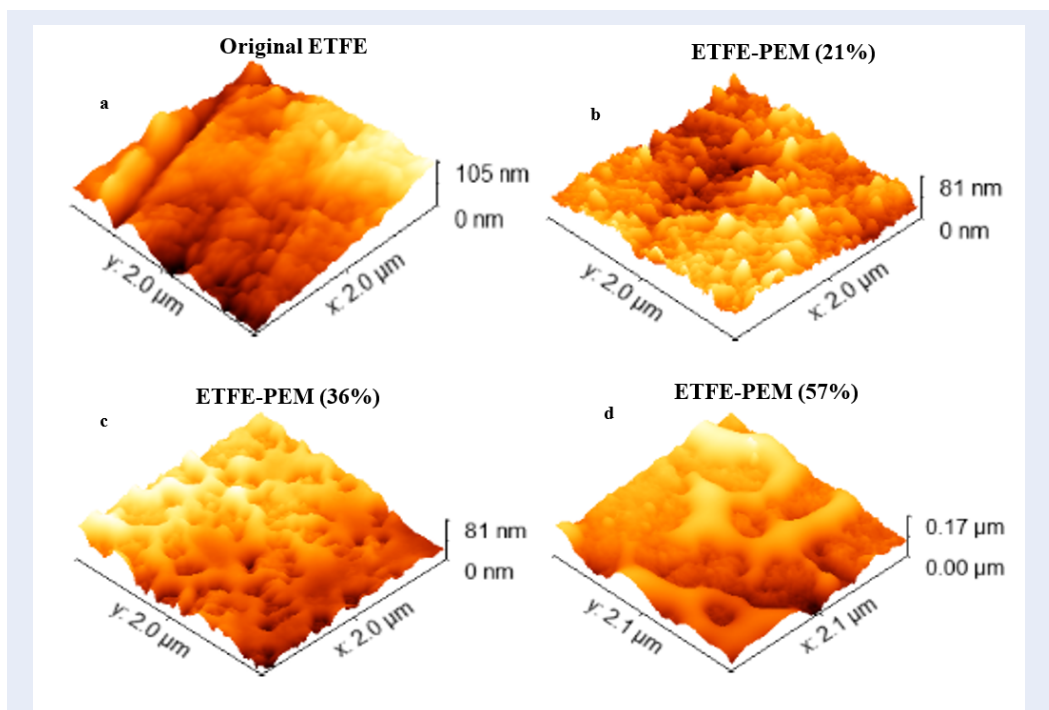


**Figure 3:** 3D surface images of the ETFE-PEMs with GDs of 0-57% at a scan size of 2000 nm. The connections among ionic domains on the membrane surface increase with the degree of grafting. In this case, the 3D image of the pristine film is also represented again for comparison.

**Table 3:** Specific surface parameters ( $S_a$ ,  $S_q$ ,  $S_z$  (P-V), and  $S_{kew}$ ) of the ETFE-PEMs with GDs of 0 - 57%. The surface parameters of the ETFE-PEMs at GDs of 21 and 36% are lower than those of the pristine ETFE film. For comparison, the specific roughness parameters of the original film are also represented again.

Sample	GD (%)	$S_a$ (nm)	$S_q$ (nm)	$S_z$ (P-V) (nm)	$S_{kew}$
Original ETFE	0	15.5	19.6	104.9	0.6
ETFE-PEM	21	10.1	12.6	81.0	0.1
ETFE-PEM	36	14.2	16.4	81.4	0.2
ETFE-PEM	57	23.3	28.3	169.1	0.2

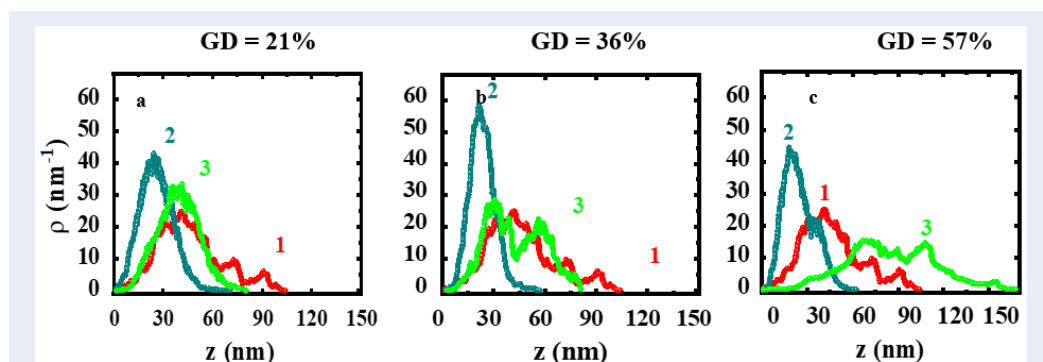


**Figure 4:** The height distribution of the samples at a scan size of 2000 nm. The original ETFE (1 – red line), grafted-ETFE (2 – cyan line), and ETFE-PEM (3 – green line) have GDs of 21–57%.

**Table 4:** Specific surface parameters ( $z$  and FWHM) of the original ETFE, grafted-ETFE, and ETFE-PEMs with GDs ranging from 21–57%. The  $z$  values of the grafted-ETFE films slightly decrease with GD, whereas those of the ETFE-PEMs increase with GD.

Sample	GD (%)	$z$ (nm)	FWHM (nm)	$R^2$
Original ETFE (peak 1)	0	40.1	35.7	0.932
Original ETFE (peak 2)	0	72.8	9.4	0.932
Grafted-ETFE	21	24.9	24.1	0.983
Grafted-ETFE	36	22.5	16.4	0.987
Grafted-ETFE	57	22.4	16.3	0.857
ETFE-PEM	21	38.9	30.4	0.985
ETFE-PEM (peak 1)	36	30.1	18.7	0.942
ETFE-PEM (peak 2)	36	56.7	21.8	0.942
ETFE-PEM (peak 1)	57	70.5	41.0	0.927
ETFE-PEM (peak 2)	57	108.7	27.8	0.927

## DISCUSSIONS

The results presented in Figure 1 and Table 1 indicate that grafting and sulfonation induced significant changes in the surface features of the grafted ETEs and ETFE-PEMs. Partially grafted PS and PSSA chains accumulate on the sample surface at a low GD of 21%. In other words, the surface features observed in Figure 1 and Table 1 reflect the partial presence of the graft chains, which are more homogeneously distributed than those of the pristine film. This result can be explained by the fact that the introduced PS chains were mostly immiscible with the amorphous phase of the pristine ETFE film, leading to the formation of a new amorphous phase containing only PS grafts<sup>5,8-10</sup>. Sulfonation results in microphase separation between the backbone of ETFE and the side chain of PSSA, but the final membrane morphology can be determined at the grafting step<sup>12,16,17</sup>. Accordingly, the surface parameters of the grafted-ETFE and ETFE-PEM (GD = 21%), represented in Table 1, are quite similar. In the case of the grafted-ETFE films, all surface parameters shown in Table 2 are lower than those of the pristine ETFE film because of the immiscibility between the PS grafts and the amorphous phase of the ETFE-based film, as mentioned above. In addition, the surface parameters do not increase with the GD, indicating that some of the PS grafts diffused into the bulk of the ETFE at the higher GD<sup>5</sup>. In particular, the  $S_a$ ,  $S_q$ , and  $S_z(P-V)$  parameters (Table 2) decrease with increasing GD from 0 to 36% and then increase again at a higher GD of 57%. This phenomenon should be related to the changes in lamellar structures reported previously<sup>16,17</sup>. Specifically, the lamellar period increases quickly from 19.1 to 25.4 nm, increases slowly from 25.4 to 28.5 nm, and then remains unchanged at approximately 28 nm within the GDs of 0–19%, 19–59%, and 59–117%, respectively. In other words, at a GD of approximately 57%, most of the graft chains were introduced out of the lamellar structures, leading to more accumulation of graft chains on the film surface, resulting in increases in the  $S_a$ ,  $S_q$ , and  $S_z(P-V)$  parameters. For the case of ETFE-PEMs, all surface parameters ( $S_a$ ,  $S_q$ , and  $S_z(P-V)$ ) shown in Table 3 are lower than those of the pristine ETFE film and grafted-ETFE films displayed in Table 2. In contrast, the values of  $S_{kew}$  for the ETFE-PEMs are lower than those for the grafted-ETFE films. Furthermore, the surface parameters (Table 3) increase with the degree of grafting, i.e., a trend dissimilar to that of the grafted ETEs (Table 2). This result reflects the effects of microphase separation, as discussed above<sup>10</sup>. In particular, the surface parameters at the GD of 57%

are significantly greater than those at the GDs of 0, 21, and 36%. This phenomenon can be elucidated similarly to that of the grafted-ETFEs at a GD of 57%. Specifically, at a GD of approximately 57%, most of the PSSA chains were generated from the lamellar stacks, leading to more accumulation of PSSA chains on the film surface, resulting in an increase in the phase separation and values of  $S_a$ ,  $S_q$ ,  $S_z(P-V)$ , and the skew parameters<sup>16,17</sup>.

The results of the height distribution shown in Figure 4 and Table 4 indicate that the PS grafts of the grafted-ETFE films are mostly immiscible within the ETFE-based matrix and can be described as a single distribution (i.e., homogeneous distribution). Moreover, the decreases in the average height (24.9–22.4 nm) and FWHM (21.1–16.3 nm) with increasing degree of grafting suggest that more PS chains diffused into the bulk of the grafted-ETFE films. This phenomenon is consistent with the 3D image features shown in Figure 2(b-d). In contrast, the PSSA grafts of ETFE-PEMs are dispersed on the membrane surface, leading to an increase in the FWHM values (Table 4). These dispersed aggregates are favorable for the connection of ionic domains, leading to larger continuous ionic domains, as observed in the 3D image features (Figure 3(b-d)). In other words, the dispersed distribution of PSSA grafts can accelerate the conductance on the membrane surface<sup>5</sup>.

## CONCLUSIONS

The surface features of the ETFE-PEMs obtained through the preparation procedure and with different degrees of grafting were investigated via TM-AFM analysis. Partially grafted PS and PSSA chains accumulated on the sample surface at a low GD of 21% and then diffused partially into the bulk of the membranes at higher GDs of 36 and 57%. All the surface parameters of the grafted-ETFE films did not clearly change with GD, whereas those of the ETFE-PEMs increased with GD. In particular, the PS grafts of the grafted-ETFE films are mostly immiscible within the ETFE-based matrix and can be described as having a single distribution (i.e., homogeneous distribution). In contrast, the PSSA grafts of ETFE-PEMs are dispersed on the membrane surface, favoring the connection of ionic domains and leading to larger continuous ionic domains. The dispersed distribution of PSSA grafts can accelerate proton conductance on the membrane surface, while the low accumulation of grafts on the membrane surface at a low GD is advantageous for improving the membrane–electrode interfacial properties of PEMFCs.



403 **LIST OF ABBREVIATIONS**

- 404 AFM: Atomic force microscopy  
 405 ETFE: Ethylene-co-tetrafluoroethylene  
 406 ETFE-PEM: Poly(styrenesulfonic acid)-grafted  
 407 poly(ethylene-co-tetrafluoroethylene) polymer  
 408 electrolyte membrane  
 409 FWHM: Full width at half maximum  
 410 GD: Grafting degree  
 411 Grafted-ETFE: Polystyrene-grafted ethylene-co-  
 412 tetrafluoroethylene  
 413 IEC: Ion exchange capacity  
 414 PEMCF: Polymer electrolyte membrane fuel cell  
 415 PS: Polystyrene  
 416 PSSA: Poly(styrenesulfonic acid)  
 417 RH: Relative humidity  
 418 TM-AFM: tapping mode atomic force microscopy

419 **COMPETING INTERESTS**

420 There are no conflicts of interest to declare.

421 **ACKNOWLEDGMENTS**

422 This work was funded by the Vingroup Big Data In-  
 423 stitute (VINBIGDATA), Vingroup and supported by  
 424 the Vingroup Innovation Foundation (VINIF) under  
 425 project code VINIF.2020.DA08.

426 **DATA AVAILABILITY STATEMENT**

427 The data sets are not publicly available but are avail-  
 428 able from the corresponding author upon reasonable  
 429 request.

430 **AUTHORS CONTRIBUTION**

431 **Tran Duy Tap:** Conceptualization, project adminis-  
 432 tration, funding acquisition, supervision, resources,  
 433 investigation, methodology, data curation, formal  
 434 analysis, supervision, validation, visualization, writ-  
 435 ing - original draft, writing - review & editing.  
 436 **Nguyen Nhat Kim Ngan:** Investigation, methodol-  
 437 ogy, data curation, formal analysis, validation, visu-  
 438 alization, writing - original draft, writing - review &  
 439 editing. **Nguyen Manh Tuan, Nguyen Huynh My**  
 440 **Tue, Vo Thi Kim Yen, Dinh Tran Trong Hieu, Hoang**  
 441 **Anh Tuan, Tran Ngoc Tien Phat, Lam Hoang Hao,**  
 442 **Nguyen Thanh Ta, Doan Thi Kim Ngan:** Investiga-  
 443 tion, Formal analysis, Visualization, Validation.

444 **REFERENCES**

445 1. Smitha B, Sridhar S, Khan AA. Solid polymer electrolyte mem-  
 446 branes for fuel cell applications - A Review. Journal of Mem-  
 447 brane Science. 2005;259(1-2):10-26;Available from: <https://doi.org/10.1016/j.memsci.2005.01.035>.  
 448  
 449 2. Hao LH, Hieu DTT, Danh TT, Long TH, Phuong HT, Luan LQ,  
 450 Man TV, Tuyen LA, Ngoc PK, Tap TD. Surface features of  
 451 polymer electrolyte membranes for fuel cell applications:

An approach using S2p XPS analysis. Science & Technology  
 Development Journal. 2021; 24(3):2100-2109;Available from:  
[https://stdj.scienceandtechnology.com.vn/index.php/stdj/  
 article/view/2556](https://stdj.scienceandtechnology.com.vn/index.php/stdj/article/view/2556).  
 452  
 453  
 454  
 455  
 3. Hao LH, Hieu DTT, Long TH, Hoa DV, Danh TT, Man TV, Luan  
 456 LQ, Phuong HT, Hong PTT, Tap TD. Investigation of the lamel-  
 457 lar grains of graft-type polymer electrolyte membranes for hy-  
 458 drogen fuel cell application using ultrasmall-angle X-ray scat-  
 459 tering. VNU Journal of Science: Natural Sciences and Techno-  
 460 logic. 2021;37:1-9;Available from: [https://doi.org/10.25073/  
 2588-1140/vnunst.5216](https://doi.org/10.25073/2588-1140/vnunst.5216).  
 461  
 462  
 4. Hao LH, Hieu DTT, Luan LQ, Phuong HT, Phuc DV,  
 463 Tuyen LA, Hong PTT, Man TV, Tap TD. Electron and gamma  
 464 irradiation-induced effects in poly(ethylene-  
 465 co-tetrafluoroethylene) films. Journal of Applied  
 466 Polymer Science. 2022;139(29):1-18;Available from:  
 467 <https://onlinelibrary.wiley.com/doi/10.1002/app.52620>.  
 468  
 469 5. Hao LH, Tap TD, Hieu DTT, Korneeva E, Tiep NV, Yoshimura  
 470 K, Hasegawa S, Sawada S, Man TV, Hung NQ, Tuyen LA,  
 471 Phuc DV, Luan LQ, Maekawa Y. Morphological characteriza-  
 472 tion of grafted polymer electrolyte membranes at a surface  
 473 layer for fuel cell application. Journal of Applied Polymer Sci-  
 474 ence. 2022;139(14):51901;Available from: [https://doi.org/10.  
 1002/app.51901](https://doi.org/10.1002/app.51901).  
 475  
 476 6. Hieu DTT, Hao LH, Danh TT, Luan LQ, Man TV, Phuong HT,  
 477 Phuc DV, Tuyen LA, Ngoc PK, Tap TD. Investigation of the  
 478 water states of poly(styrene sulfonic acid) (PSSA) grafted  
 479 poly(ethylene-co-tetrafluoroethylene) copolymer using FT-IR  
 480 analysis, Vietnam Journal of Science, Technology and Engi-  
 481 neering. 2022;64:3-9;Available from: [https://doi.org/10.31276/  
 VJSTE.64\(2\).03-09](https://doi.org/10.31276/VJSTE.64(2).03-09).  
 482  
 483 7. Hieu DTT, Hao LH, Long TH, Tien VV, Cuong NT, Man TV, Loan  
 484 TTH, Tap TD. Investigation of chemical degradation and water  
 485 states in the graft-type polymer electrolyte membranes. Poly-  
 486 mer Engineering and Science. 2022;62: 2757-2768;Available  
 487 from: <https://doi.org/10.1002/pen.26059>.  
 488  
 489 8. Long TH, Hieu DT, Hao LH, Cuong NT, Loan TTH, Man TV,  
 490 Tap DT. Positron annihilation lifetime spectroscopic analy-  
 491 sis of Nafion and graft-type polymer electrolyte membranes  
 492 for fuel cell application. Polymer Engineering and Science.  
 493 2022;62:4005-4017;Available from: [https://doi.org/10.1002/  
 pen.26162](https://doi.org/10.1002/pen.26162).  
 494  
 495 9. Tap TD, Long TH, Hieu DT, Hao LH, Phuong HT, Luan LQ, Mann  
 496 TV. Positron annihilation lifetime study of subnano level free  
 497 volume features of grafted polymer electrolyte membranes  
 498 for hydrogen fuel cell applications. Polymers for Advanced  
 499 Technologies. 2022;33:2952-2965;Available from: [https://doi.  
 org/10.1002/pat.5761](https://doi.org/10.1002/pat.5761).  
 500  
 501 10. Tap TD, Hasegawa S, Yoshimura K, Yen VTK, Tue NH, Tuan NM,  
 502 Hieu DTT, Tuan HA, Hao LH, Nguyen LL, Phuong HT, Luan LQ,  
 503 Man TV, Maekawa Y. Phase separation and water channels in  
 504 graft-type polymer electrolyte membranes for hydrogen fuel  
 505 cell. International Journal of Hydrogen Energy. 2024;59:777-  
 506 790;Available from: [https://doi.org/10.1016/j.ijhydene.2024.02.  
 082](https://doi.org/10.1016/j.ijhydene.2024.02.082).  
 507  
 508 11. Tap TD, Nguyen LL, Hien NQ, Thang PB, Sawada SI, Hasegawa  
 509 S, Maekawa Y. Humidity and temperature effects on me-  
 510 chanical properties and conductivity of graft-type poly-  
 511 mer electrolyte membrane. Radiation Physics and Chemistry.  
 512 2018;151:186-191;Available from: [https://doi.org/10.1016/j.  
 radphyschem.2018.06.033](https://doi.org/10.1016/j.radphyschem.2018.06.033).  
 513  
 514 12. Tuan NM, Tue NH, Yen VTK, Ngan NNK, Hieu DTT, Tuan HA,  
 515 Huy DQ, Tap TD. Features of ionic domains in graft-type  
 516 polymer electrolyte membranes using small angle X-ray scat-  
 517 tering analysis. Science & Technology Development Jour-  
 518 nal. 2024;27:1-13;Available from: [https://doi.org/10.32508/  
 stdj.v26i4.4052](https://doi.org/10.32508/stdj.v26i4.4052).  
 519  
 520 13. Tue NHM, Long TH, Hieu DTT, Hao LH, Yen VTK, Tuan NM,  
 521 Phuong HT, Luan LQ, Hong PTT, Man TV, Tap TD. Effects of  
 522 source correction in positron annihilation lifetime spectro-  
 scopic analysis of graft-type polymer electrolyte membranes.

- 523 Science & Technology Development Journal. 2023;26:3060-  
524 3068;Available from: <https://doi.org/10.32508/stdj.v26i4.4052>.
- 525 14. Yen VTK, Hieu DTT, Hao LH, Long TH, Tue NHM, Tuan NM,  
526 Cuong NT, Loan TTH, Man TV, Tap TD. Characterization of  
527 graft-type polymer electrolyte membrane at low grafting de-  
528 gree for fuel cell. Science & Technology Development Jour-  
529 nal. 2023;26(2):2799-2807;Available from: <https://doi.org/10.32508/stdj.v26i2.4051>.
- 530 15. Tap TD, Sawada SI, Hasegawa S, Katsumura Y, Maekawa  
531 Y. Poly (ethylene-co-tetrafluoroethylene)(ETFE)-based graft-  
532 type polymer electrolyte membranes with different ion ex-  
533 change capacities: Relative humidity dependence for fuel  
534 cell applications. Journal of Membrane Science. 2013;447:19-  
535 25;Available from: <https://doi.org/10.1016/j.memsci.2013.07.041>.
- 536 16. Tap TD, Sawada S, Hasegawa S, Yoshimura K, Oba Y, Ohnuma  
537 M, Katsumura Y, Maekawa Y. Hierarchical structure–property  
538 relationships in graft-type fluorinated polymer electrolyte  
539 membranes using small- and ultrasmall-angle X-ray scattering  
540 analysis. Macromolecules. 2014;47(7):2373-2383;Available  
541 from: <https://doi.org/10.1021/ma500111x>.
- 542 17. Tap TD, Nguyen LL, Zhao Y, Hasegawa S, Sawada SI,  
543 Hung NQ, Maekawa Y. SAXS investigation on morpho-  
544 logical change in lamellar structures during propagation  
545 steps of graft-type polymer electrolyte membranes for fuel  
546 cell applications. Macromolecular Chemistry and Physics.  
547 2020;221(3):1900325;Available from: <https://doi.org/10.1002/macp.201900325>.
- 548 18. Tap TD, Nguyen LL, Hasegawa S, Sawada SI, Luan LQ, Maekawa  
549 Y. Internal and interfacial structure analysis of graft-type flu-  
550 orinated polymer electrolyte membranes by small-angle X-  
551 ray scattering in the high q range. Journal of Applied Poly-  
552 mer Science. 2020;137(35):49029;Available from: <https://doi.org/10.1002/app.49029>.
- 553 19. Nagy G, Sproll V, Gasser U, Schmidt TJ, Gubler L, Ba-  
554 log S. Scaling the graft length and graft density of  
555 irradiation-grafted copolymers. Macromolecular Chem-  
556 istry and Physics. 2018;219(21):1800311;Available from:  
557 <https://doi.org/10.1002/macp.201800311>.
- 558 20. Sproll V, Schmidt TJ, Gubler L. Grafting design: A strat-  
559 egy to increase the performance of radiation-grafted mem-  
560 branes. Polymer International. 2016;65(2):174-180;Available  
561 from: <https://doi.org/10.1002/pi.5041>.
- 562 21. Gürsel SA, Schneider J, Ben Youcef H, Wokaun A,  
563 Scherer GG. Thermal properties of proton-conducting  
564 radiation-grafted membranes. Journal of Applied Poly-  
565 mer Science. 2008;108(6):3577-3585;Available from:  
566 <https://doi.org/10.1002/app.27947>.
- 567 22. Hatanaka T, Hasegawa N, Kamiya A, Kawasumi M, Mori-  
568 moto Y, Kawahara K. Cell performances of direct methanol  
569 fuel cells with grafted membranes. Fuel 2002;81(17):2173-  
570 2176;Available from: [https://doi.org/10.1016/S0016-2361\(02\)00164-3](https://doi.org/10.1016/S0016-2361(02)00164-3).
- 571 23. Sherazi TA, Guiver MD, Kingston D, Ahmad S, Kashmiri MA,  
572 Xue X. Radiation-grafted membranes based on polyethy-  
573 lene for direct methanol fuel cells. Journal of Power Sources  
574 2010;195(1):21-29;Available from: <https://doi.org/10.1016/j.jpowsour.2009.07.021>.
- 575 24. Nasef MM, Saidi H, Ambar M. Cation exchange mem-  
576 branes by radiation-induced graft copolymerization of  
577 styrene onto PFA copolymer films. IV. Morphological in-  
578 vestigations using X-ray photoelectron spectroscopy.  
579 Journal of Applied Polymer Science. 2000;77:2455;Available  
580 from: [https://onlinelibrary.wiley.com/doi/abs/10.1002/1097-4628\(20000912\)77:11%3C2455::AID-APP14%3E3.0.CO;2-5](https://onlinelibrary.wiley.com/doi/abs/10.1002/1097-4628(20000912)77:11%3C2455::AID-APP14%3E3.0.CO;2-5).
- 581 25. Nasef MM, Saidi H. Postmortem analysis of Journal of ap-  
582 plied polymer science radiation grafted fuel cell membrane  
583 using X-ray photoelectron spectroscopy. Journal of New  
584 Materials for Electrochemical Systems 2002;5:183;Avail-  
585 able from: [https://eprints.utm.my/3714/1/Nasef2002\\_Post-  
586 morteAnalysisRadiationGraftedFuel.pdf](https://eprints.utm.my/3714/1/Nasef2002_Post-morteAnalysisRadiationGraftedFuel.pdf).
- 587 26. Nasef MM, Saidi H, Nor HM, Yarmo MA. XPS studies of radiation  
588 grafted PTFE-g-polystyrene sulfonic acid membranes. Journal  
589 of applied polymer science 2000;76:336;Available from:  
590 [https://onlinelibrary.wiley.com/doi/abs/10.1002/\(SICI\)1097-4628\(20000418\)76:3%3C336::AID-APP9%3E3.0.CO;2-E](https://onlinelibrary.wiley.com/doi/abs/10.1002/(SICI)1097-4628(20000418)76:3%3C336::AID-APP9%3E3.0.CO;2-E).
- 591 27. Nasef MM, Saidi H, Nor HM, Foo OM. Proton ex-  
592 change membranes prepared by simultaneous radia-  
593 tion grafting of styrene onto poly(tetrafluoroethylene-  
594 co-hexafluoropropylene) films. II. Properties of sul-  
595 fonated membranes. Journal of applied polymer science  
596 2000;78:2443;Available from: [https://onlinelibrary.wiley.com/doi/abs/10.1002/1097-4628\(20001227\)78:14%3C2443::AID-APP30%3E3.0.CO;2-E](https://onlinelibrary.wiley.com/doi/abs/10.1002/1097-4628(20001227)78:14%3C2443::AID-APP30%3E3.0.CO;2-E).
- 597 28. Gubler L, Prost N, Gürsel SA, Scherer GG. Proton ex-  
598 change membranes prepared by radiatingrafting  
599 of styrene/divinylbenzene onto poly(ethylene-alt-  
600 tetrafluoroethylene) for low temperaturefuel cells. Solid  
601 State Ionics. 2005;176:2849;Available from: <https://www.sciencedirect.com/science/article/abs/pii/S0167273805004686>.
- 602 29. Giessibl FJ. Advances in atomic force microscopy. Reviews  
603 of Modern Physics. 2003;75(3):949;Available from: <https://doi.org/10.1103/RevModPhys.75.949>.
- 604 30. Webb HK, Truong VK, Hasan J, Fluke C, Crawford RJ,  
605 Ivanova EP. Roughness parameters for standard descrip-  
606 tion of surface nanoarchitecture. Scanning. 2012;34(4):257-  
607 263;Available from: <https://doi.org/10.1002/sca.21002>.
- 608 31. Nečas D, Klapetek P. Gwyddion: an open-source software  
609 for SPM data analysis. Central European Journal of Physics.  
610 2012;10(1):181-188;Available from: <https://doi.org/10.2478/s11534-011-0096-2>.
- 611 32. Motegi T, Yoshimura K, Zhao Y, Hiroki A, Maekawa  
612 Y. Direct observation and semiquantitative analy-  
613 sis of hierarchical structures in graft-type polymer  
614 electrolyte membranes using the AFM technique.  
615 Langmuir. 2022;38(32):9992-9999;Available from:  
616 <https://pubs.acs.org/doi/abs/10.1021/acs.langmuir.2c01398>.
- 617 33. Spreitzer H, Kaufmann B, Ruzié C, Röthel C, Arnold T, Geerts  
618 YH, Teichert C, Resel R, Jones AO. Alkyl chain assisted thin film  
619 growth of 2,7-dioctyloxy-benzothienobenzothiophene. Jour-  
620 nal of Materials Chemistry C. 2019;7(27):8477-8484;Available  
621 from: <https://doi.org/10.1039/C9TC01979K>.
- 622 623 624 625 626 627 628 629 630 631 632 633 634